Apoptosis (2024) 29:920–933
https://doi.org/10.1007/s10495-024-01946-5

hP-MSCs attenuate severe acute pancreatitis in mice via inhibiting NLRP3 inflammasome-mediated acinar cell pyroptosis

Shuang Lyu[1,2,3] · Shuirong Liu[2] · Xin Guo[2] · Yaolei Zhang[2] · Zhongyu Liu[4] · Shan Shi[2] · Wenya Li[2] · Juan Pei[1,2] · Yonghong Fan[1,2] · Hongyu Sun[1,2,3]

Accepted: 13 February 2024 / Published online: 16 April 2024

Abstract

Background Severe acute pancreatitis (SAP) is a serious gastrointestinal disease that is facilitated by pancreatic acinar cell death. The protective role of human placental mesenchymal stem cells (hP-MSCs) in SAP has been demonstrated in our previous studies. However, the underlying mechanisms of this therapy remain unclear. Herein, we investigated the regularity of acinar cell pyroptosis during SAP and investigated whether the protective effect of hP-MSCs was associated with the inhibition of acinar cell pyroptosis.

Methods A mouse model of SAP was established by the retrograde injection of sodium taurocholate (NaTC) solution in the pancreatic duct. For the hP-MSCs group, hP-MSCs were injected via the tail vein and were monitored in vivo. Transmission electron microscopy (TEM) was used to observe the pyroptosis-associated ultramorphology of acinar cells. Immunofluorescence and Western blotting were subsequently used to assess the localization and expression of pyroptosis-associated proteins in acinar cells. Systemic inflammation and local injury-associated parameters were evaluated.

Results Acinar cell pyroptosis was observed during SAP, and the expression of pyroptosis-associated proteins initially increased, peaked at 24 h, and subsequently showed a decreasing trend. hP-MSCs effectively attenuated systemic inflammation and local injury in the SAP model mice. Importantly, hP-MSCs decreased the expression of pyroptosis-associated proteins and the activity of the NOD-, LRR-, and pyrin domain-containing protein 3 (NLRP3) inflammasome in acinar cells.

Conclusions Our study demonstrates the regularity and important role of acinar cell pyroptosis during SAP. hP-MSCs attenuate inflammation and inhibit acinar cell pyroptosis via suppressing NLRP3 inflammasome activation, thereby exerting a protective effect against SAP.

Keywords Severe acute pancreatitis · Acinar cells · Pyroptosis · Human placental mesenchymal stem cells · NLRP3 inflammasome

Introduction

Severe acute pancreatitis (SAP) is a serious gastrointestinal disease with a mortality risk as high as 20.0%∼50.0% and is characterized by systemic inflammation and local injury [1–3]. During SAP, the release of inflammatory mediators tends to trigger systemic inflammatory response syndrome (SIRS), potentially leading to multiple-organ dysfunction syndrome (MODS) and even fatal outcomes [1, 3]. Current management strategies for SAP mainly include goal-directed fluid resuscitation, appropriate enteral nutritional support, and the targeted use of therapeutic agents [4]. Although these clinical strategies have been used in patients with SAP, the prevention and treatment of SAP remain major challenges.

Shuang Lyu and Shuirong Liu contributed equally to this work.

✉ Yonghong Fan
yhfan@foxmail.com

✉ Hongyu Sun
shongyu2008@163.com

[1] College of Medicine, Southwest Jiaotong University, Chengdu, Sichuan 610031, China

[2] Laboratory of Basic Medicine, The General Hospital of Western Theater Command, Chengdu, Sichuan 610083, China

[3] General Surgery Center of PLA and Pancreatic Injury and Repair Key Laboratory of Sichuan Province, The General Hospital of Western Theater Command, Chengdu, Sichuan 610083, China

[4] School of Clinical Medicine, Southwest Medical University, Luzhou, Sichuan 646000, China

Mesenchymal stem cells (MSCs) are a class of pluripotent stem cells that offer new potential therapeutic options for the treatment of patients with inflammatory diseases due to their low immunogenicity and remarkable immunomodulatory properties [5–7]. Many studies have shown obvious protective effects of MSCs, including human placenta-derived mesenchymal stem cells (hP-MSCs), human umbilical cord-derived mesenchymal stem cells (hUC-MSCs), and human adipose tissue-derived mesenchymal stem cells (hAT-MSCs), against SAP [8–10]. Our previous study confirmed that hP-MSCs exerted a beneficial effect on SAP rats via inducing the M2 polarization of macrophages [8]. In addition, another study by Li et al. showed that hAT-MSCs ameliorated SAP in mice via decreasing endoplasmic reticulum (ER) stress [10]. Although some progress has been made in recent years, the underlying mechanism behind the therapeutic effect of MSCs has not been fully elucidated.

Pancreatic acinar cells are among the major functional cells involved in the exocrine division of the pancreas. Acinar cell death can arise from a series of pathological intra-acinar events, subsequently leading to pancreatic injury and systemic inflammation [11, 12]. Among regulated cell death (RCD) events, pyroptosis is a form of RCD that can promote inflammation and lysis. Its biochemical features include the formation of inflammasomes and the activation of inflammatory caspases and gasdermin family members [13, 14]. Pyroptosis can be induced through either the caspase-1-dependent signaling pathway or the caspase-1-independent signaling pathway. Activated caspase-1 can further convert pro-interleukin-1β (IL-1β) and pro-interleukin-18 (IL-18) into their mature forms. Moreover, the N-terminal domain (NTD) of gasdermin D (GSDMD) is cleaved, leading to oligomerization and the formation of pores in cytomembranes and subsequently to inflammatory cell death accompanied by the loss of cytomembrane integrity and the release of inflammatory mediators [13–16]. Wang et al. demonstrated that the activation of the NOD-, LRR-, and pyrin domain-containing protein 3 (NLRP3) inflammasome and caspase-1 induced acinar cell pyroptosis and inflammatory cytokine secretion to aggravate acute pancreatitis (AP) [17]. In addition, Gao et al. reported that acinar cell pyroptosis, pancreatic necrosis, and systemic inflammation were significantly reduced in AP mice with acinar cell conditional *Gsdmd* inhibition and that the protection against AP was further enhanced by the combination of RIP3 inhibitors in *Gsdmd*$^{-/-}$ mice [18]. These data indicate that inhibiting acinar cell pyroptosis is a potential therapeutic strategy for AP. However, the effect of hP-MSCs on acinar cell pyroptosis in SAP has not been determined.

Based on the findings described above, we systematically evaluated the regularity of acinar cell pyroptosis during SAP and determined whether the protective effect of hP-MSCs was associated with inhibiting acinar cell pyroptosis. The findings of this study will contribute to a deeper understanding of the underlying mechanisms involved in stem cell therapy for SAP.

Materials and methods

Ethics statement

This study was approved by the Ethics Committee of the General Hospital of Western Theater Command of the Chinese People's Liberation Army (2021EC2-20). All mice were housed in a specific pathogen-free (SPF) laboratory animal environment at 23.0 °C ± 3.0 °C with 55.0% ± 5.0% relative humidity and under a 12-h light/dark cycle, and they had free access to potable water and standard chow. Throughout the experiments, the researchers strictly followed the Principles of Laboratory Animal Care (revised in 1996) published by the National Institutes of Health of the United States of America and the Animal Management Regulations (revised in 2017) issued by the National Science and Technology Commission of the People's Republic of China to minimize animal suffering and the number of animals used during the experiments. After the experiments, all animals were killed in a scientific and regulated manner.

Materials

Adipogenesis-, osteogenesis-, and chondrogenesis-induced differentiation kits and surface marker assay kits specialized for MSCs were purchased from Cyagen Biotechnology Co., Ltd. (Guangdong, PRC). Serum-free medium and recombinant trypsin solution specialized for MSCs were purchased from Yocon Biology Technology Company Co., Ltd. (Beijing, PRC). SPF male C57BL/6 mice (weighing 22 g ± 2 g) were purchased from Sipeifu (Beijing) Biotechnology Co., Ltd. (Beijing, PRC). Sodium taurocholate (NaTC) was purchased from Sigma-Aldrich Chemie GmbH (Taufkirchen, GER). 1,1'-Dioctadecyl-3,3,3',3'-tetramethylindotricarbocyanine iodide (DiR) was purchased from MedChemExpress, LLC (New Jersey, USA). An amylase mouse enzyme-linked immunosorbent assay (ELISA) kit and a lipase mouse ELISA kit were purchased from Jiangsu Meimian Industrial Co., Ltd. (Jiangsu, PRC). A tumor necrosis factor-α (TNF-α) mouse ELISA kit, interleukin-6 (IL-6) mouse ELISA kit, interleukin-4 (IL-4) mouse ELISA kit, and interleukin-10 (IL-10) mouse ELISA kit were purchased from Thermo Fisher Scientific, Inc. (Massachusetts, USA). A hematoxylin and eosin (H&E) staining kit was purchased from Shanghai Beyotime Biotechnology Co., Ltd. (Shanghai, PRC). Anti-NLRP3, anti-caspase-1, anti-GAPDH, goat anti-rabbit IgG

H&L (HRP), goat anti-rabbit IgG H&L (Alexa Fluor 488), and donkey anti-rabbit IgG H&L (Alexa Fluor 555) antibodies were purchased from Abcam, PLC (Cambridge, UK). An anti-GSDMD antibody was purchased from ABclonal Technology Co., Ltd. (Hubei, PRC). Anti-apoptosis-associated speck-like protein containing a caspase-recruitment domain (ASC) and anti-IL-1β antibodies were purchased from Cell Signaling Technology, Inc. (Massachusetts, USA). An anti-amylase antibody was purchased from Proteintech Group, Inc. (Illinois, USA).

Culture and characterization of hP-MSCs

The details of the hP-MSCs are described in a previous study by Huang et al. [19]. The hP-MSCs were cultured in mesenchymal stem cell-specific serum-free medium under suitable conditions at 37.0 °C, 21.0% O_2 and 5.0% CO_2. Subculture was performed when the cells reached 80.0% ~ 90.0% confluence, and hP-MSCs between the 3rd and 6th passages were selected for experiments. For the characterization of hP-MSCs, hP-MSCs were first observed morphologically using a microscope. Second, hP-MSCs were further assessed for adipogenesis, osteogenesis, and chondrogenesis under appropriate culture conditions. Finally, flow cytometry was used to detect the surface-specific antigens of hP-MSCs, including CD11b, CD29, CD14, CD44, CD45, CD34, CD73, CD105, CD166, and HLA-DR.

Animals

Throughout the surgical procedure, the researchers strictly followed the principle of aseptic technique. To avoid adverse gastrointestinal reactions during the perioperative period, all the mice were fasted 6 h before surgery. The animal surgical room was irradiated with ultraviolet light (ultraviolet radiation intensity > 120.0 μW/cm^2) 2 h before surgery, and the relevant surgical instruments were sterilized using autoclave steam (0.14 MPa, 126.0 °C, 30 min) before use. Isoflurane vapor was inhaled for induction (2.5%, v/v) and maintenance (1.5%, v/v) of anesthesia in all mice during surgery.

All mice were randomly divided into a sham group, SAP group, and hP-MSCs group. In the sham group, anesthetized mice were fixed in the supine position on an operating table, and their abdominal skin was later prepared and disinfected with iodophor (1.0%, w/v). After the abdominal wall of the mouse was incised along the anterior midline of the abdomen, the pancreas was turned over several times with a sterile cotton swab, after which the abdominal cavity was closed. After closure of the abdominal cavity, 0.1 mL of PBS solution was injected into the mice via the tail vein 0 and 6 h postsurgery. In the SAP group, after the abdominal cavity was opened as described above, the mice were retrogradely injected with 4.0% (w/v) NaTC solution (1.0 mL/kg of bw, 0.1 mL/min) in the pancreatic duct using a microinjection pump, after which the abdominal cavity was closed. After the abdominal cavity was closed, the same volume of PBS solution was injected via the tail vein as described above. In the hP-MSCs group, each mouse was injected with an hP-MSCs suspension (5.0×10^6 cells/kg of bw) via the tail vein 0 and 6 h after model establishment as described above.

Appropriate numbers of mice in each group were killed 12 h, 24 h, 36 h, and 48 h after model establishment, and blood, pancreas, and lung samples were properly collected and preserved for subsequent experiments. The experimental procedure is shown in the schematic illustration in Fig. 4A.

In vivo tracing of hP-MSCs

The hP-MSCs were labeled with the fluorescent probe DiR according to the manufacturer's protocol.

For in vivo tracing, a DiR-labeled hP-MSCs suspension was injected into SAP model mice (5.0×10^6 cells/kg of bw) via the tail vein 0 and 6 h after model establishment. Specifically, the distribution of hP-MSCs in SAP model mice over time was traced using a small animal imaging system 0 h before the first injection and 12 h, 24 h, 36 h, and 48 h after the first injection.

Survival assessment

All mice were housed in a suitable living environment after surgery and had free access to potable water and standard chow. Moreover, the survival of the mice in each group was recorded at specific time points. In this study, events such as mice killed for subsequent experiments and died from abnormalities like death by an incision split were considered censoring.

ELISA

Blood samples were centrifuged for 15 min at 4.0 °C and 1,800 × *g*, after which the serum was collected. Subsequently, the activities of amylase and lipase and the concentrations of TNF-α, IL-6, IL-4, and IL-10 in the serum were measured using the appropriate ELISA kits according to the manufacturers' protocols.

Pathological examination

After the mice were killed, they were fixed in the supine position on an operating table, and then, the abdominal skin was disinfected with 1.0% iodophor solution. Subsequently,

the abdominal wall of each mouse was incised along the anterior midline of the abdomen, and the pancreas tissues were fully exposed and observed visually for edema, hemorrhage and other gross pathological changes.

For histopathological examination, fresh pancreas and lung tissues were fixed with 4.0% paraformaldehyde solution, treated with a concentration gradient of ethanol and xylene, and embedded in paraffin. Sections (4 μm thick) were prepared, deparaffinized, rehydrated and stained with H&E. Subsequently, the histopathological scores of the pancreas and lung sections were performed blindly by two pathologists following the criteria reported by Schmidt et al. and Hu et al., respectively [20, 21].

Measurement of the wet/dry weight ratio

The wet weights of the fresh pancreas and lung tissues were determined using an electronic balance and recorded. The fresh tissues were then dried for 72 h at 80.0 °C. After drying, the dry weights of the pancreas and lung tissues were again measured using an electronic balance, and the results were recorded. The wet/dry weight ratio was calculated as the wet weight of the fresh tissue divided by the dry weight of the dried tissue.

Transmission electron microscopy (TEM) imaging

Fresh pancreas tissues were sequentially prefixed with 3.0% glutaraldehyde solution, fixed with 1.0% osmium tetroxide solution, dehydrated with a concentration gradient of acetone, and embedded in Epon812 to make semithin sections and subsequent ultrathin sections with a thickness of 70 nm. Subsequently, the ultrathin sections were placed on 200-mesh copper grids, stained with uranyl acetate and lead citrate solution and then observed by a transmission electron microscope at 80 kV.

Western blotting

Total protein was extracted from fresh pancreas tissues with a whole protein extraction kit, after which protein quantification was performed with a protein assay kit, and protein denaturation was performed with loading buffer in preparation for subsequent protein experiments. All relevant steps were carried out according to the manufacturers' protocols. Equal amounts of sample were electrophoresed in sodium dodecyl sulfate-polyacrylamide gels, followed by transfer of the proteins separated on the sodium dodecyl sulfate-polyacrylamide gels to methanol–saturated polyvinylidene difluoride membranes and subsequent blocking of the polyvinylidene difluoride membranes for 1 h with blot blocking buffer at room temperature. For protein immunoblotting, polyvinylidene difluoride membranes were co-incubated overnight at 4.0 °C with the following primary antibodies: anti-NLRP3 antibody (1/1,000 dilution), anti-ASC antibody (1/1,000 dilution), anti-caspase-1 antibody (1/1,000 dilution), anti-GSDMD antibody (1/2,000 dilution), anti-IL-1β antibody (1/1,000 dilution), and anti-GAPDH antibody (1/5,000 dilution). The next day, the polyvinylidene difluoride membranes were washed three times with Tris-buffered saline containing Tween-20 (TBST), and the polyvinylidene difluoride membranes were co-incubated for 1 h at room temperature with the following secondary antibody: goat anti-rabbit IgG H&L (HRP) antibody (1/10,000 dilution). After incubation, the polyvinylidene difluoride membranes were washed three additional times with TBST, and the bands were subsequently visualized with diaminobenzidine and imaged using a gel imaging system. Finally, the intensity of the target protein bands was analyzed semi-quantitatively using ImageJ.

Immunofluorescence

For immunofluorescence, deparaffinized and rehydrated sections were heated in citrate buffer (pH = 6.0) for 10 min for antigen retrieval. Then, the sections were washed three times with Phosphate-buffered saline containing Tween-20 (PBST), after which the sections were blocked for 1 h with 5.0% serum solution at room temperature, permeabilized with 0.2% Triton X-100 solution and washed three times with PBST. After performing the relevant procedures as described above, the sections were co-incubated overnight at 4.0 °C with the following primary antibodies: anti-NLRP3 antibody (1/50 dilution), anti-caspase-1 antibody (1/50 dilution), and anti-GSDMD antibody (1/100 dilution). The next day, the sections were washed three times with PBST and co-incubated for 1 h away from light at room temperature with the following secondary antibody: donkey anti-rabbit IgG H&L (Alexa Fluor 555) antibody (1/500 dilution). Subsequently, the sections were sequentially co-incubated according to the process described above away from light with the following antibodies: anti-amylase antibody (1/50 dilution) and goat anti-rabbit IgG H&L (Alexa Fluor 488) antibody (1/500 dilution) 4,6-Diamino-2-phenyl indole (DAPI) was used to identify the nuclei of the cells. After incubation, the sections were washed three additional times with PBST, and the images were taken under a fluorescence microscope. Finally, the images were analyzed semi-quantitatively using ImageJ.

Statistical analysis

All the data in this study were statistically analyzed using GraphPad Prism 9.5.0 and IBM SPSS Statistics 26.0. The

product-limit method (Kaplan-Meier method) was used to describe the survival process, and the log-rank test was used to perform survival analysis. The measurement data are expressed as the mean ± standard error of the mean (SEM) and were subjected to normality and homogeneity of variance tests. The Kruskal-Wallis test was used when the data did not conform to a normal distribution, one-way analysis of variance (ANOVA) was used when the data conformed to a normal distribution and exhibited homoscedasticity, and Welch's ANOVA was used when the data conformed to a normal distribution but did not exhibit homoscedasticity. Differences were considered statistically significant when P was < 0.05.

Results

The ultrastructural injury to acinar cells tends to increase during SAP

As shown in Fig. 1A, the pancreas from mice in the SAP group at different time points exhibited varying degrees of edema and hemorrhage, while the gross morphology and color of the pancreas of mice in the sham group were normal. In addition, compared with the sham group, the SAP group at different time points showed increased structural disorganization of the pancreas with more interlobular edema, necrosis of acinar cells, and hemorrhage (Fig. 1B and C). Pancreatic injury was further assessed by measuring serum amylase and lipase activities. The two biochemical parameters were significantly increased in the SAP group (Fig. 1D). These data demonstrate a mouse model of SAP successfully established by the retrograde injection of 4.0% (w/v) NaTC solution in the pancreatic duct.

Then, TEM was used to observe the ultramicroscopic morphological features of the acinar cells. As shown in Fig. 1E and F, the acinar cells from mice in the SAP group at different time points exhibited significant pathological features. Specifically, as time progressed, zymogen granules (ZG) accumulated. Pore formation increased, causing the cytomembrane to lose its integrity and rupture. The morphology of the ER changed, and cystic dilation gradually occurred. Moreover, the mitochondria (Mi) were swollen, and their ridges appeared lysed and fractured. In contrast, the acinar cells from mice in the sham group were morphologically normal and contained evenly distributed ZG. The cytomembrane was structurally intact, and organelles such as the ER and Mi were morphologically normal. These results indicate that ultrastructural injury tends to be aggravated in acinar cells during SAP.

Pyroptosis is activated in acinar cells during SAP

Given the critical importance of acinar cell pyroptosis for systemic inflammation and pancreatic injury during SAP, the localization and expression of pyroptosis-associated proteins were examined. Immunofluorescence showed that the caspase-1 and GSDMD signals were mainly localized in the cytoplasm of acinar cells. Furthermore, at different time points, these signal intensities were more intense in the SAP group than in the sham group, and the signal intensities peaked at 24 h (Fig. 2A and B). Importantly, the NLRP3 signal was also localized mainly in the cytoplasm of acinar cells. Similarly, at different time points, this signal intensity was more intense in the SAP group than in the sham group, and the signal intensity peaked at 24 h (Fig. 2C and D).

Western blot analysis revealed that the expression of pyroptosis-associated proteins in the pancreas was significantly greater in the SAP group than in the sham group at different time points. More importantly, the expression of pyroptosis-associated proteins peaked at 24 h and remained high at 48 h (Fig. 3A and B). Considering that pyroptosis triggers the activation of intracellular pro-IL-1β and the release of its activated form, we further examined the levels of pro-IL-1β and cleaved IL-1β in the pancreas. As shown in Fig. 3C and D, the levels of pro-IL-1β and cleaved IL-1β in the pancreas in the SAP group were significantly greater at different time points than those in the sham group and peaked at 24 h. In particular, the expression of NLRP3 and ASC in the pancreas in the SAP group was significantly upregulated at different time points compared with that in the sham group, peaking at 24 h and remaining high at 48 h (Fig. 3E and F). These findings indicate that acinar cells undergo pyroptosis during SAP.

hP-MSCs colonize the injured pancreas

We characterized hP-MSCs previously and investigated the ability of hP-MSCs to be used for in vivo tracing and homing in SAP model mice. As shown in Fig. S1A, hP-MSCs exhibited a swirling arrangement and typical fibroblast-like morphology during culture. Subsequently, hP-MSCs were further subjected to three-lineage induction differentiation to examine their differentiation ability. The results show that hP-MSCs retain the ability to differentiate into adipogenic, osteogenic, and chondrogenic lineages (Fig. S1B, C, and D). Importantly, the surface-specific antigens of hP-MSCs were analyzed to assess their phenotypic characteristics. As shown in Fig. S1E, these cells were positive for CD29, CD44, CD73, CD105, and CD166 but negative for CD11b, CD14, CD34, CD45, and HLA-DR.

Then, we injected DiR-labeled hP-MSCs into SAP model mice via the tail vein and observed their biodistribution in

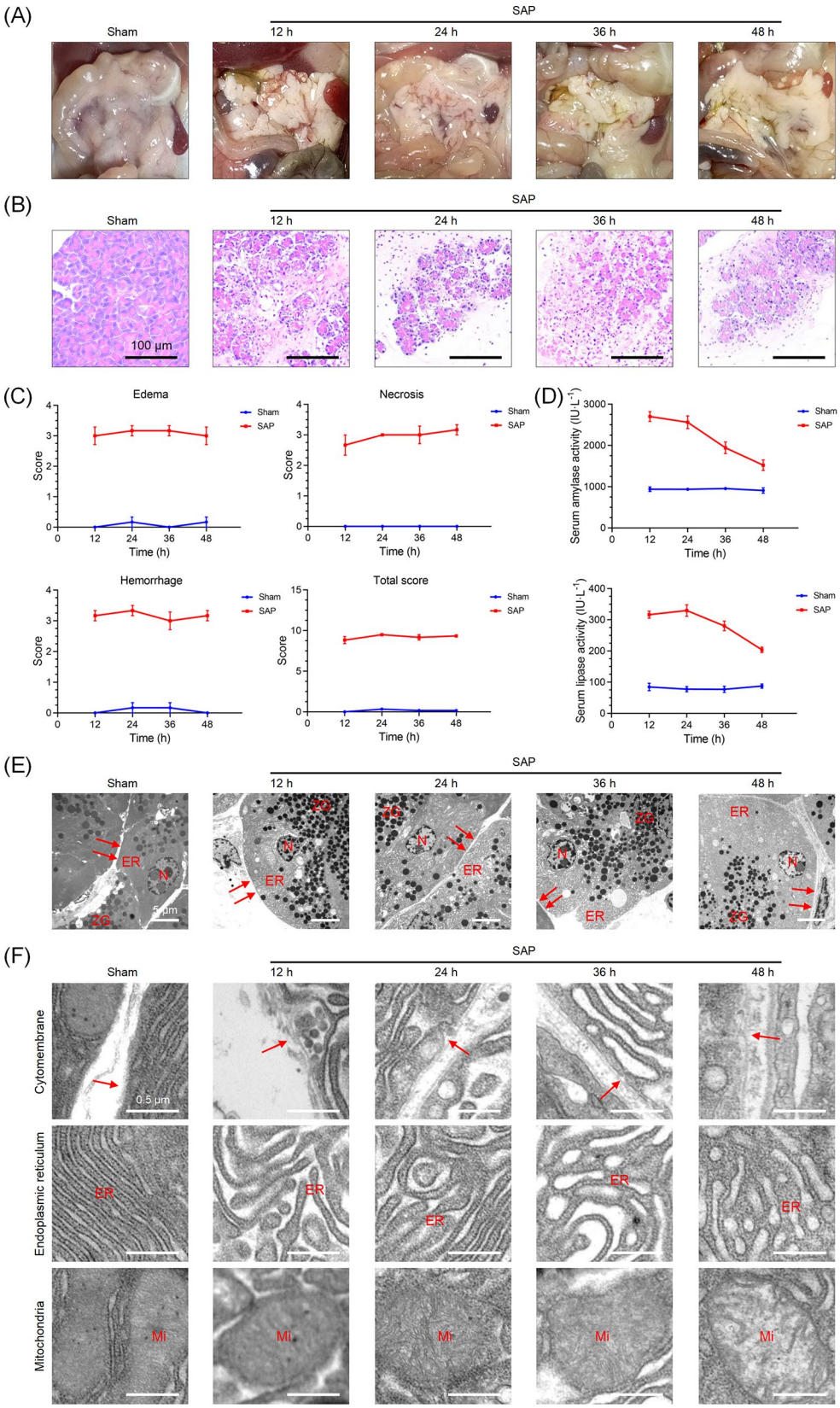

Fig. 1 The ultrastructural injury to acinar cells tends to be aggravated during SAP. (**A**) Gross morphology images of the pancreas from mice in the sham group and the SAP group at different time points. $n = 3$ per group. (**B** and **C**) Histopathologic images and pathological scores for the pancreas tissues from mice in the sham group and the SAP group at different time points. Scale bar = 100 μm. $n = 3$ per group. (**D**) Serum amylase and lipase activities in mice in the sham group and the SAP group at different time points. $n = 3$ per group. (**E**) TEM images of local acinar cells from mice in the sham group and the SAP group at different time points. Zymogen granules (ZG), cytomembrane (red arrow), nucleus (N), endoplasmic reticulum (ER) and mitochondria (Mi) are shown in these images. Scale bar = 5 μm. $n = 3$ per group. (**F**) TEM images of the cytomembrane and major organelles of acinar cells from mice in the sham group and the SAP group at different time points. The cytomembrane (red arrow), endoplasmic reticulum (ER) and mitochondria (Mi) are shown in these images. Scale bar = 0.5 μm. $n = 3$ per group. (**C** and **D**) Data are expressed as the mean ± SEM

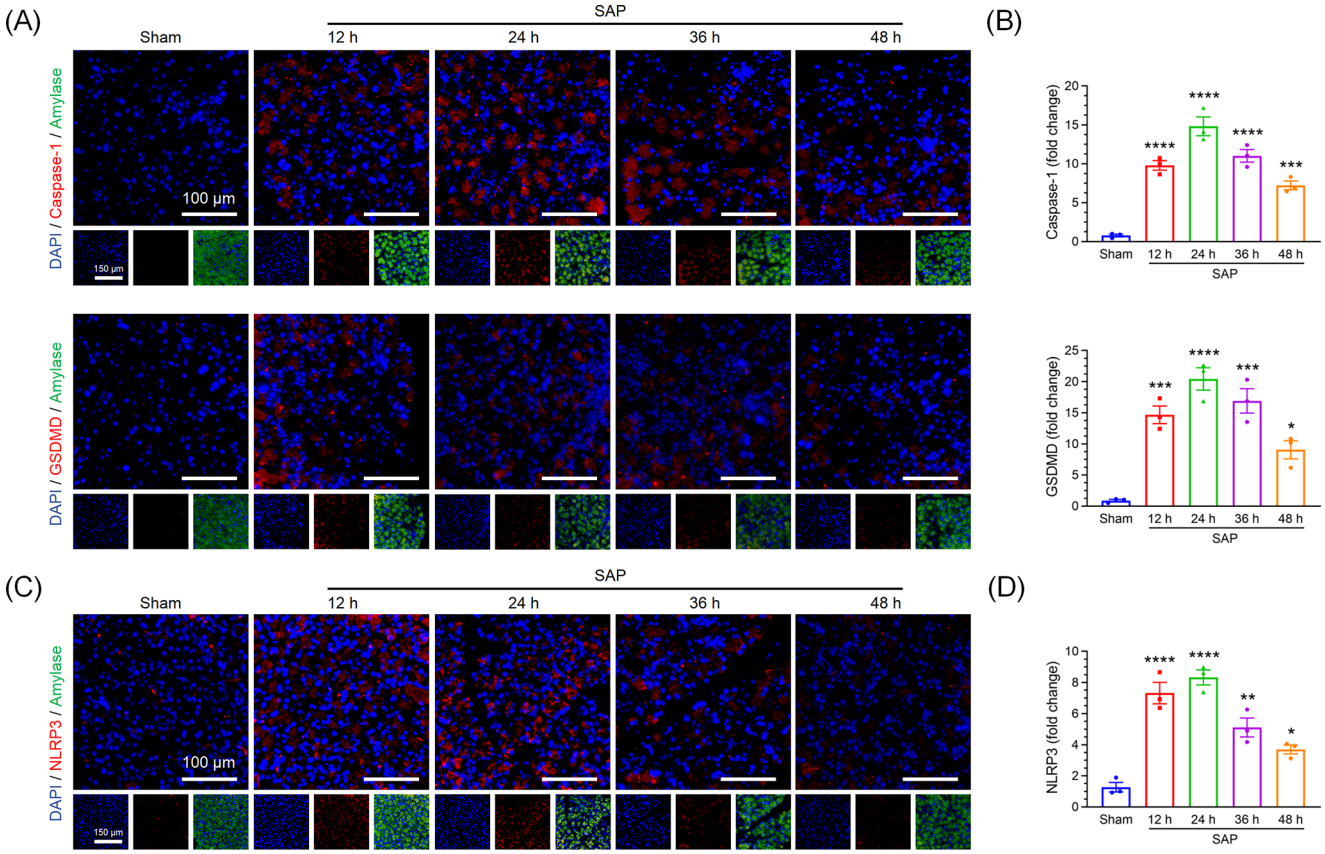

Fig. 2 Pyroptosis is activated in acinar cells during SAP. (**A** and **B**) Immunofluorescence images and statistical analysis of caspase-1 and GSDMD in acinar cells from mice in the sham group and the SAP group at different time points. The tricolor fluorescence signals are red (caspase-1 or GSDMD), green (amylase), and blue (nucleus). Scale bar = 100 μm. Associate images are presented. scale bar = 150 μm. $n = 3$ per group. (**C** and **D**) Immunofluorescence images and statistical analysis of NLRP3 in acinar cells from mice in the sham group and the SAP group at different time points. The tricolor fluorescence signals are red (NLRP3), green (amylase), and blue (nucleus). Scale bar = 100 μm. Associate images are presented. scale bar = 150 μm. $n = 3$ per group. (**B** and **D**) Data are expressed as the mean ± SEM. $^{*}P < 0.05$ versus the sham group, $^{**}P < 0.01$ versus the sham group, $^{***}P < 0.001$ versus the sham group, and $^{****}P < 0.0001$ versus the sham group

vivo at different time points. The fluorescent signals were mainly distributed in the abdominal and thoracic cavities of SAP model mice and that their intensity decreased over time (Fig. 4B and C). The fluorescence signal intensity of DiR-labeled hP-MSCs was greater than that of DiR (Fig. 4D, E, and F). Moreover, fluorescent signals accumulated mainly in the pancreas, lungs, liver, and spleen 12 h after the first injection of DiR-labeled hP-MSCs. Fluorescent signals were mainly distributed in the pancreas, liver, and lungs 48 h after the first injection of DiR-labeled hP-MSCs, but the intensity of the corresponding fluorescence signals decreased (Fig. 4G and H). These data demonstrate that hP-MSCs colonize the injured pancreas during SAP. To investigate the role of hP-MSCs in SAP and acinar cell pyroptosis, we selected 24 h as the time point for a more detailed study.

hP-MSCs attenuate systemic inflammation and local injury in SAP

Systemic inflammation and local organ injury are two characteristic features of SAP, and we next sought to determine the effect of hP-MSCs on these two features. First, 48-h survival was observed. As shown in Fig. 5A, dead mouse individuals began to occur 2 h after model establishment in the SAP group and 1 h after that in the hP-MSCs group. The 48-h survival of mice in the hP-MSCs group was significantly greater than that in the SAP group. Serum TNF-α, IL-6, IL-4, and IL-10 levels were examined to assess systemic inflammation. Compared with mice in the sham group, mice in the SAP group had significantly higher serum concentrations of TNF-α and IL-6 but significantly lower serum concentrations of IL-10 and IL-4. Moreover, hP-MSCs significantly decreased the serum concentrations of TNF-α and IL-6 but increased the serum concentration of

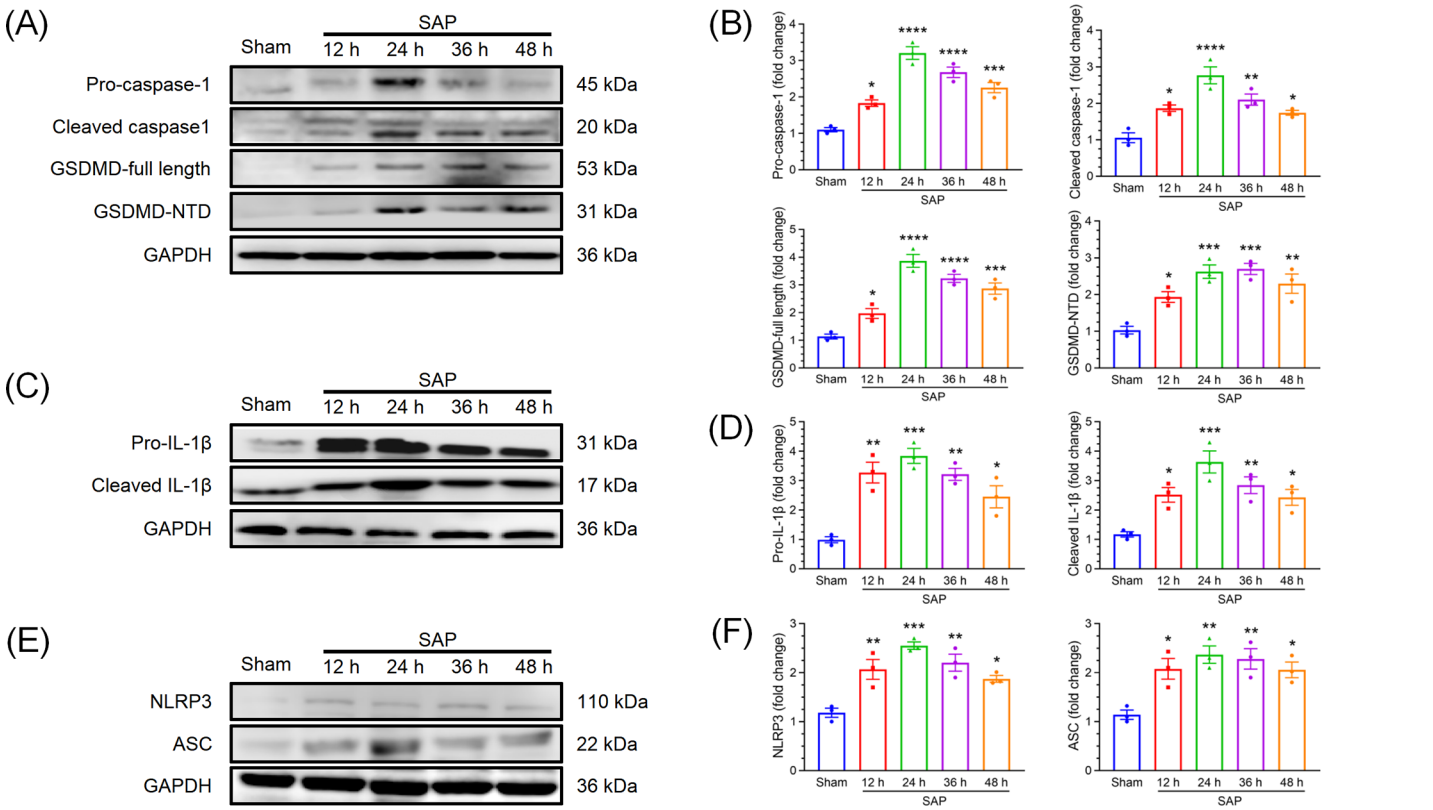

Fig. 3 Pyroptosis is activated in the pancreas during SAP. (**A** and **B**) Western blot images and statistical analysis of pro-caspase-1, cleaved caspase-1, GSDMD-full length, and GSDMD-NTD in the pancreas from mice in the sham group and the SAP group at different time points. $n = 3$ per group. (**C** and **D**) Western blot images and statistical analysis of pro-IL-1β and cleaved IL-1β in the pancreas from mice in the sham group and the SAP group at different time points. $n = 3$ per group. (**E** and **F**) Western blot images and statistical analysis of NLRP3 and ASC in the pancreas from mice in the sham group and the SAP group at different time points. $n = 3$ per group. (**B**, **D** and **F**) Data are expressed as the mean ± SEM. $^{*}P < 0.05$ versus the sham group, $^{**}P < 0.01$ versus the sham group, $^{***}P < 0.001$ versus the sham group, and $^{****}P < 0.0001$ versus the sham group

IL-10. However, hP-MSCs did not change the serum concentration of IL-4 (Fig. 5B).

Pancreatic injury was then assessed by examining serum amylase and lipase activities. Both biochemical parameters were significantly lower in the hP-MSCs group than in the SAP group (Fig. 5C). To better understand the role of hP-MSCs, we analyzed the micropathology of the pancreas and lung tissues. Compared with the SAP group, the hP-MSCs group showed reduced structural disorganization of the pancreas with less interlobular edema, necrosis of acinar cells, and hemorrhage (Fig. 5D and E). Since lung injury is a common complication of SAP, we next examined whether hP-MSCs ameliorated lung injury in SAP model mice. Compared with the SAP group, the hP-MSCs group exhibited improved structural disorganization and significant reductions in edema, inflammatory cell infiltration, and hemorrhage (Fig. 5F and G). The wet/dry weight ratios of the pancreas and lung tissues were measured to further evaluate edema. Compared with those in the SAP group, the degree of pancreas and lung tissue edema in the hP-MSCs group was lower (Fig. 5H). Furthermore, TNF-α and IL-6 levels in the pancreas were significantly lower in the hP-MSCs group than in the SAP group (Fig. 5I). These results indicate that hP-MSCs effectively alleviate systemic inflammation and local pancreatic injury in SAP model mice.

hP-MSCs alleviate pyroptosis-associated ultrastructural injury to acinar cells in SAP

We sought to determine whether the protective effect of hP-MSCs was associated with the inhibition of acinar cell pyroptosis. TEM imaging revealed that the degree of injury to acinar cells was significantly lower in the hP-MSCs group than in the SAP group and that the number of accumulated ZG was lower in the hP-MSCs group than in the SAP group (Fig. 6A). Specifically, compared with those in the SAP group, the number of cytomembrane pores in the hP-MSCs group was lower. In addition, compared with the SAP group, in the hP-MSCs group, there was a lower degree of ER dilatation and Mi swelling (Fig. 6B). Immunofluorescence revealed that the signal intensities for caspase-1 and GSDMD in the hP-MSCs group were lower than those in

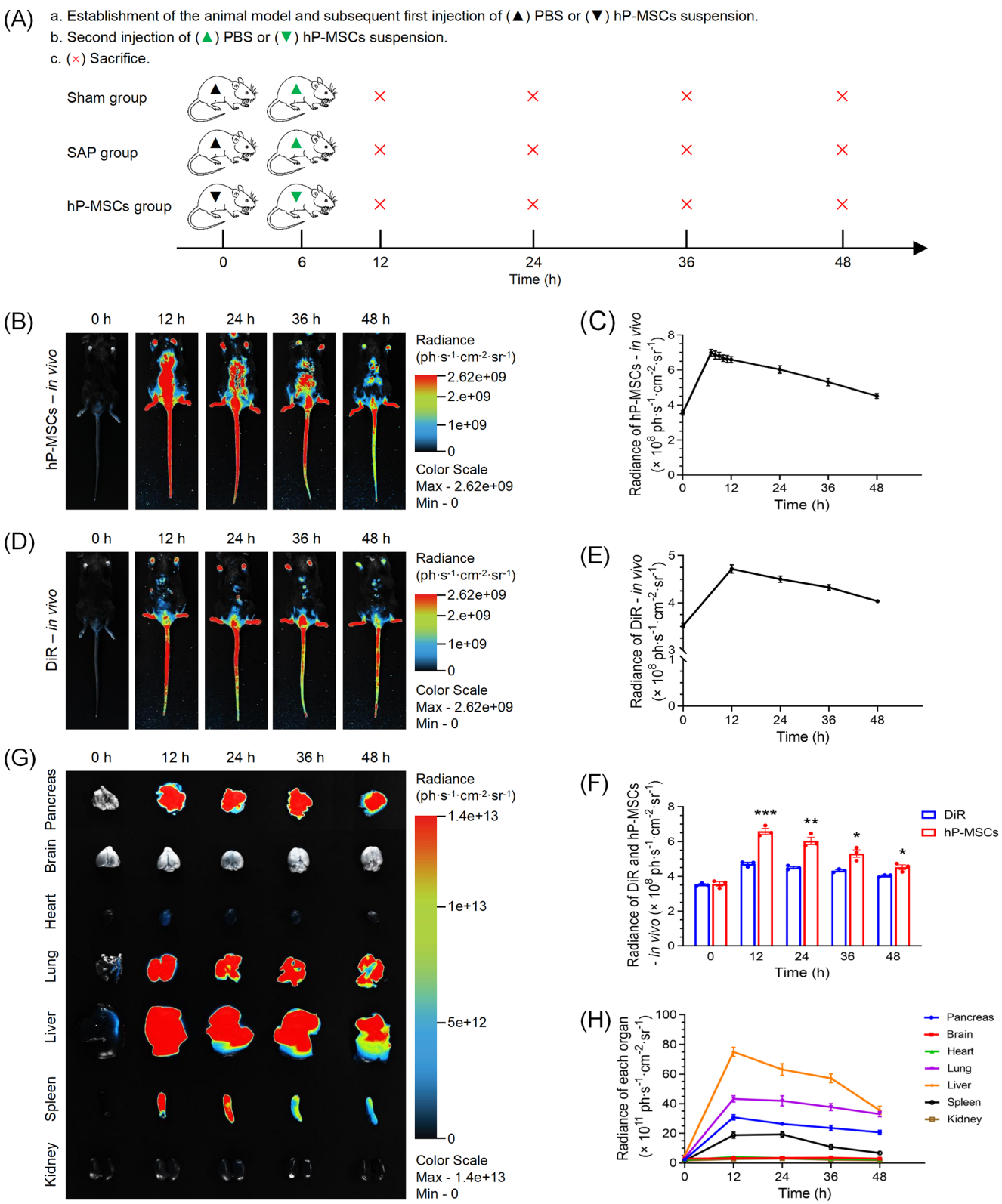

Fig. 4 hP-MSCs colonize the injured pancreas and other major organs in SAP model mice. (**A**) Schematic illustration of the animal experimental procedure. (**B** and **C**) in vivo tracing images and statistical analysis of DiR-labeled hP-MSCs at different time points. $n=3$ per group. (**D** and **E**) in vivo tracing images and statistical analysis of DiR at different time points. $n=3$ per group. (**F**) Radiance for in vivo tracing of DiR-labeled hP-MSCs and DiR at different time points. $n=3$ per group. $^{*}P<0.05$ versus the DiR group, $^{**}P<0.01$ versus the DiR group, $^{***}P<0.001$ versus the DiR group. (**G** and **H**) Fluorescence images and statistical analysis of DiR-labeled hP-MSCs in the pancreas, brain, heart, lung, liver, spleen, and kidney at different time points. $n=3$ per group. (**C**, **E**, **F**, and **H**) Data are expressed as the mean ± SEM

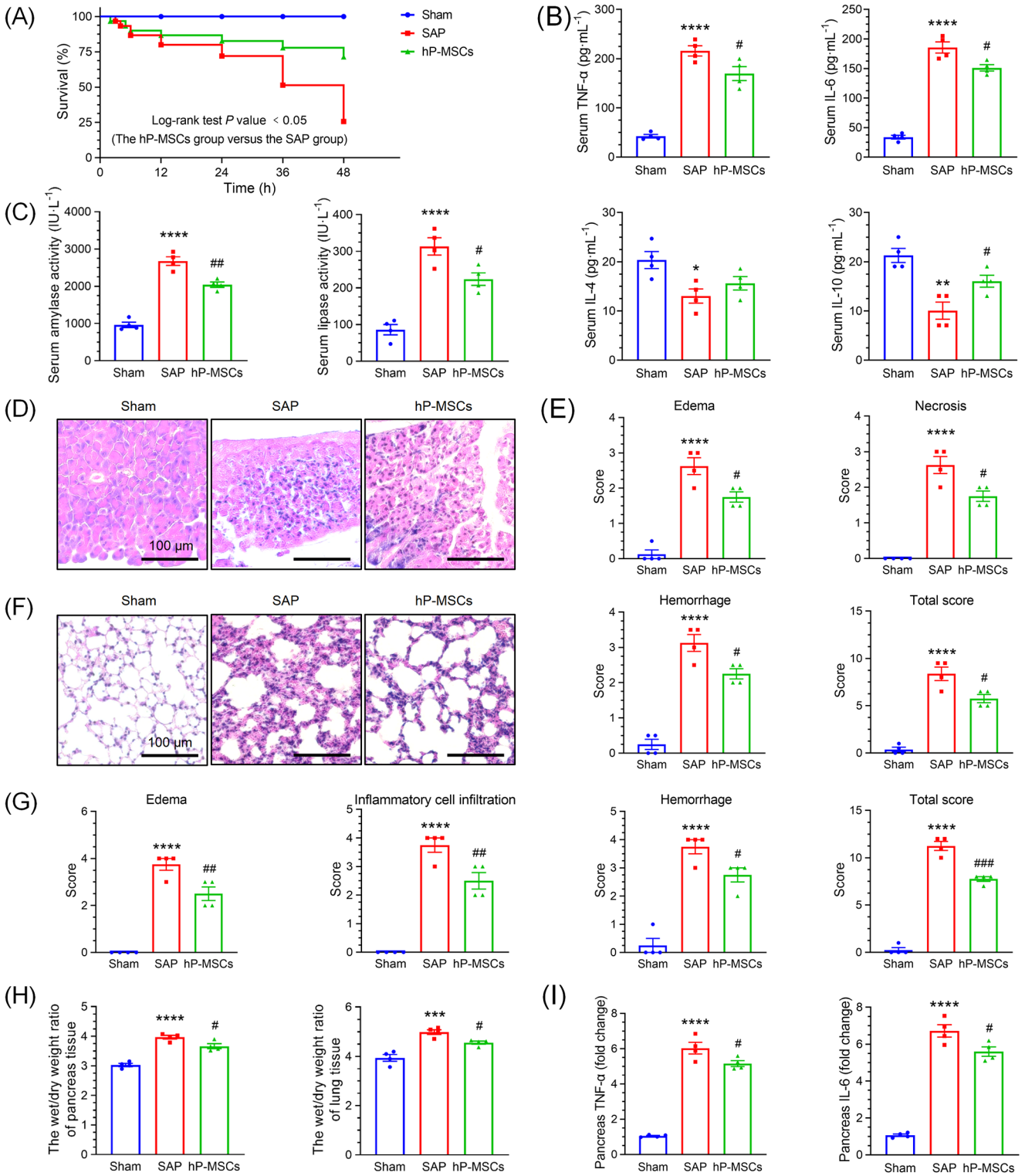

Fig. 5 hP-MSCs attenuate systemic inflammation and local injury in SAP model mice. (**A**) Cumulative survival of mice in each group from model establishment to 48 h after model establishment. $n = 30$ per group. (**B**) TNF-α, IL-6, IL-4, and IL-10 levels in the serum from mice in each group. $n = 4$ per group. (**C**) Serum amylase and lipase activities in the mice in each group. $n = 4$ per group. (**D** and **E**) Histopathologic images and pathological scores for the pancreas tissues from mice in each group. Scale bar = 100 μm. $n = 4$ per group. (**F** and **G**) Histopathologic images and pathological scores for the lung tissues from mice in each group. Scale bar = 100 μm. $n = 4$ per group. (**H**) The wet/dry weight ratios of the pancreas and lung tissues from mice in each group. $n = 4$ per group. (**I**) TNF-α and IL-6 levels in the pancreas from mice in each group. $n = 4$ per group. (**B**, **C**, **E**, **G**, **H**, and **I**) Data are expressed as the mean ± SEM. $^{*}P < 0.05$ versus the sham group, $^{**}P < 0.01$ versus the sham group, $^{***}P < 0.001$ versus the sham group, $^{****}P < 0.0001$ versus the sham group, $^{\#}P < 0.05$ versus the SAP group, $^{\#\#}P < 0.01$ versus the SAP group, and $^{\#\#\#}P < 0.001$ versus the SAP group

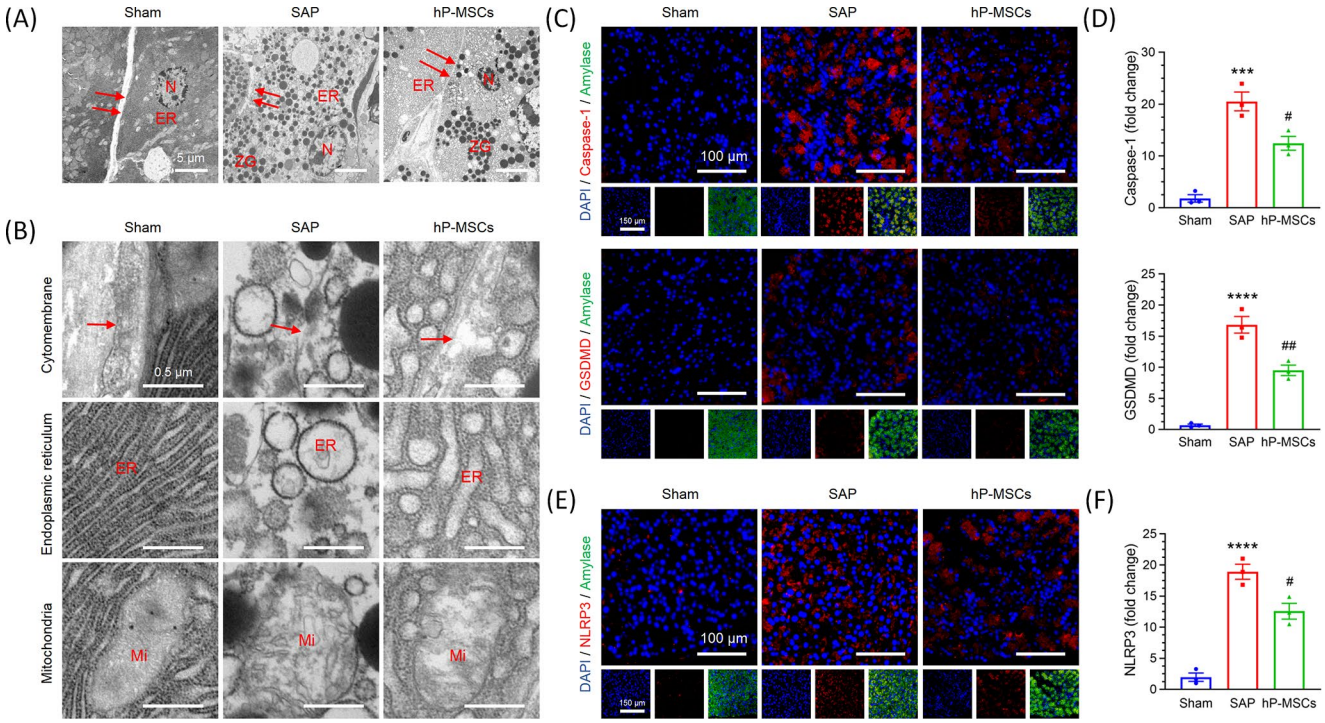

Fig. 6 hP-MSCs alleviate pyroptosis-associated ultrastructural injury to acinar cells in SAP model mice. (**A**) TEM images of local acinar cells from mice in each group. Zymogen granules (ZG), cytomembrane (red arrow), nucleus (N), endoplasmic reticulum (ER) and mitochondria (Mi) are shown in these images. Scale bar = 5 μm. $n = 3$ per group. (**B**) TEM images of the cytomembrane and major organelles of acinar cells from mice in each group. The cytomembrane (red arrow), endoplasmic reticulum (ER) and mitochondria (Mi) are shown in these images. Scale bar = 0.5 μm. $n = 3$ per group. (**C** and **D**) Immunofluorescence images and statistical analysis of caspase-1 and GSDMD in acinar cells from mice in each group. The tricolor fluorescence signals are red (caspase-1 or GSDMD), green (amylase), and blue (nucleus). Scale bar = 100 μm. Associate images are presented. scale bar = 150 μm. $n = 3$ per group. (**E** and **F**) Immunofluorescence images and statistical analysis of NLRP3 in cells from mice in each group. The tricolor fluorescence signals are red (NLRP3), green (amylase), and blue (nucleus). Scale bar = 100 μm. Associate images are presented. scale bar = 150 μm. $n = 3$ per group. (**D** and **F**) Data are expressed as the mean ± SEM. $^{***}P < 0.001$ versus the sham group, $^{****}P < 0.0001$ versus the sham group, $^{\#}P < 0.05$ versus the SAP group, and $^{\#\#}P < 0.01$ versus the SAP group

the SAP group (Fig. 6C and D). Importantly, compared with the SAP group, the hP-MSCs group exhibited significantly less signal intensity for NLRP3 (Fig. 6E and F). These findings indicate that hP-MSCs attenuate ultrastructural injury and decrease the expression of caspase-1, GSDMD, and NLRP3 in acinar cells.

hP-MSCs inhibit NLRP3 inflammasome-mediated pyroptosis in SAP

We then examined the effect of hP-MSCs on the expression of pyroptosis-associated proteins in the pancreas. Western blot analysis revealed that the expression of pyroptosis-associated proteins was significantly lower in the hP-MSCs group than in the SAP group (Fig. 7A and B). The hP-MSCs group showed significantly lower levels of pro-IL-1β and cleaved IL-1β than did the SAP group (Fig. 7C and D). In particular, the expression of NLRP3 and ASC in the hP-MSCs group was significantly lower than that in the SAP group (Fig. 7E and F). Overall, the above results demonstrate that hP-MSCs inhibit acinar cell pyroptosis via suppressing NLRP3 inflammasome activation in SAP model mice.

Discussion

In this study, we explore the regularity of acinar cell pyroptosis during SAP and the protective role and mechanism of action of hP-MSCs in SAP. The main findings include the following: (I) acinar cell pyroptosis initially increases, with a peak at 24 h, and subsequently decreases during SAP, (II) hP-MSCs attenuate systemic inflammation parameters and pancreatic injury and inhibit acinar cell pyroptosis in SAP model mice, and (III) the protective role of hP-MSCs in SAP may be associated with the inhibition of the NLRP3 inflammasome-mediated pyroptosis pathway. Taken together, our results indicate that hP-MSCs exert a protective effect via inhibiting NLRP3 inflammasome-mediated acinar cell pyroptosis.

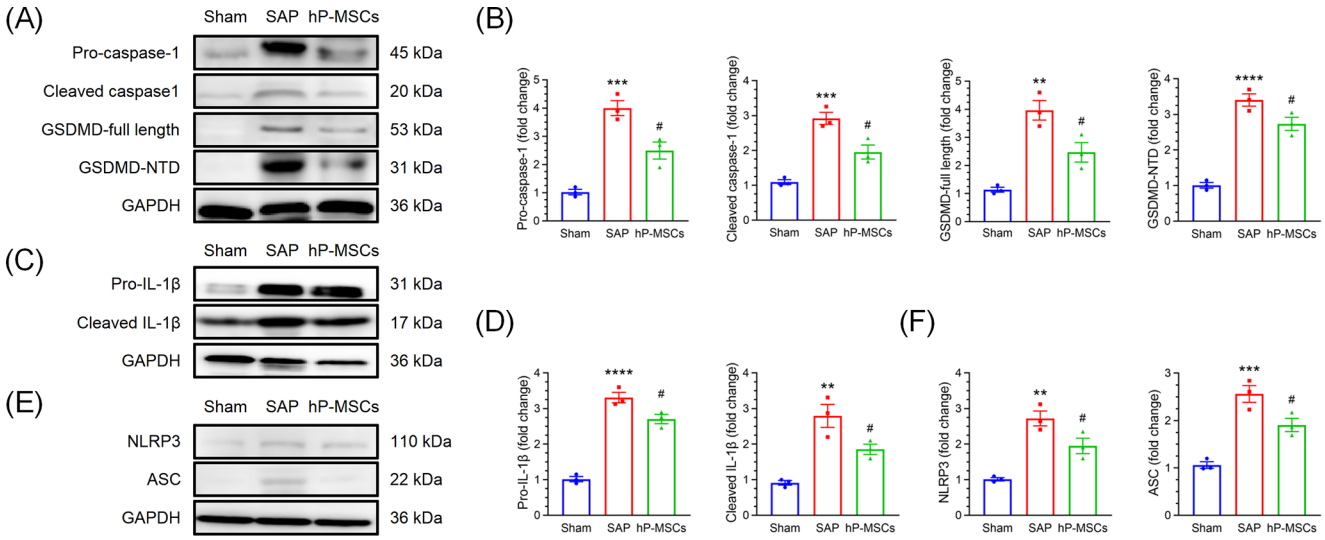

Fig. 7 hP-MSCs inhibit NLRP3 inflammasome-mediated pyroptosis in SAP model mice. (**A** and **B**) Western blot images and statistical analysis of pro-caspase-1, cleaved caspase-1, GSDMD-full length, and GSDMD-NTD in the pancreas from mice in each group. $n=3$ per group. (**C** and **D**) Western blot images and statistical analysis of pro-IL-1β and cleaved IL-1β in the pancreas from mice in each group. $n=3$ per group. (**E** and **F**) Western blot images and statistical analysis of NLRP3 and ASC in the pancreas from mice in each group. $n=3$ per group. (**B**, **D**, and **F**) Data are expressed as the mean ± SEM. $^{**}P<0.01$ versus the sham group, $^{***}P<0.001$ versus the sham group, $^{****}P<0.0001$ versus the sham group, and $^{\#}P<0.05$ versus the SAP group

Pyroptosis is a novel form of RCD that serves as an important natural immune response and plays an important role in responses to exogenous and endogenous danger signals [13, 22]. As protein molecules involved in pyroptosis, caspase-1 and GSDMD play important roles in exacerbating AP [23]. It has been reported that the inhibition of caspase-1 reduces the secretion of proinflammatory cytokines and the occurrence of acinar cell pyroptosis in AP and attenuates the severity of AP [17]. In addition, Wang et al. showed that the activation of GSDMD promoted acinar cell pyroptosis to exacerbate AP [24]. However, how pyroptosis changes in acinar cells during SAP is not fully understood. Our study reveals that the expression of pyroptosis-associated proteins in the SAP group is significantly greater than that in the sham group and is mainly localized in the cytoplasm of acinar cells, which is consistent with the findings of Gao et al. [18]. Importantly, we found that the expression of pyroptosis-associated proteins tended to increase initially, peaking at 24 h, decreasing afterward and remaining high at 48 h. Additionally, the activation and release of IL-1β are downstream effects of activated caspase-1 and pore formation in the cytomembrane [25]. In our study, the levels of pro-IL-1β and activated IL-1β in the SAP group were also significantly greater than those in the sham group. Moreover, the expression of these proteins peaked at 24 h and remained high at 48 h. Thus, acinar cell pyroptosis might result in increased systemic inflammation and local injury in SAP. These findings suggest that acinar cell pyroptosis plays an important role in SAP. Therefore, inhibiting pyroptosis may be a potential therapeutic strategy for the treatment of SAP.

Numerous studies have shown that MSCs have immunomodulatory and anti-inflammatory effects on various diseases [26, 27]. The ways in which MSCs exert therapeutic effects are multifaceted and include inducing the differentiation of multiple cell types and exerting paracrine effects through various bioactive mediators [28]. There is increasing evidence that MSCs colonize immunomodulatory organs and injured tissues to decrease inflammatory cascades and exert reparative effects [29–32]. In this study, we found that the fluorescence signal intensity in the pancreas of SAP model mice significantly increased after the injection of hP-MSCs. These data suggest that hP-MSCs colonize the injured pancreas in SAP model mice, which may be an important basis for the therapeutic effects of hP-MSCs. In addition, we also found that hP-MSCs colonized organs such as the lungs and liver. SAP often leads to inflammatory injuries, such as SAP-associated lung or liver injury, and the injured tissues may chemoattract MSCs for colonization [33, 34]. Taking the lungs as an example, possible reasons for these tissue effects are the rich blood flow in the lungs and a capillary diameter smaller than MSCs. Therefore, when MSCs are infused intravenously, most colonize the lungs through a process called the pulmonary first-pass effect [35].

More recently, several studies have shown that MSCs exert therapeutic or protective effects by regulating pyroptosis in many inflammatory diseases [36–38]. Acinar cell pyroptosis is an important component of the promotion of pancreatic inflammation and plays a crucial role in driving SAP. However, whether the protective effect of hP-MSCs

against SAP is associated with the inhibition of acinar cell pyroptosis is unknown. We systematically evaluated the influence of hP-MSCs on acinar cell pyroptosis in SAP model mice. Our study reveals that hP-MSCs significantly inhibit the expression of pyroptosis-associated proteins and decrease the level of IL-1β in SAP model mice. In this study, for the first time, we explored that hP-MSCs significantly inhibited the pyroptosis of acinar cells and attenuated a variety of inflammatory parameters in SAP model mice. These data are highly important for revealing the mechanism by which hP-MSCs attenuate SAP.

Furthermore, we investigated the potential mechanism by which MSCs inhibit acinar cell pyroptosis in SAP. Inflammasomes are molecular platforms for caspase-1 activation and are assembled from self-oligomerizing scaffold proteins. Inflammasome-dependent caspase-1 activation results in a highly inflammatory form of pyroptosis [39]. NLRP3 is an intracellular sensor that detects a wide range of endogenous danger signals and environmental irritants. When NLRP3 is stimulated by the pathological signals described above, NLRP3 inflammasomes form and are activated [40]. Several studies have reported that MSCs inhibit pyroptosis via suppressing NLRP3 inflammasome activation in inflammatory diseases [41, 42]. Our study indicates that hP-MSCs inhibit the pyroptosis of acinar cells in SAP via suppressing NLRP3 inflammasome activation. These data provide new insights into the mechanism by which hP-MSCs inhibit acinar cell pyroptosis in SAP.

There are several limitations in our study. The exact mechanism by which hP-MSCs inhibit NLRP3 inflammasome-mediated pyroptosis in SAP is unknown and needs to be further explored. In addition, we investigated the inhibitory effect of hP-MSCs on acinar cell pyroptosis in SAP only in vivo, and therefore, the corresponding in vitro experiments will be investigated in our future work.

Conclusions

In summary, the results of this study demonstrate that acinar cell pyroptosis tends to increase initially and then decrease, an effect that be related to the progression of SAP. Notably, hP-MSCs inhibit acinar cell pyroptosis and attenuate inflammation in SAP model mice via suppressing NLRP3 inflammasome activation, thereby exerting a protective effect against SAP. Although the underlying mechanisms still need to be explored in depth, these results provide important evidence that hP-MSCs exert a protective effect against acinar cell pyroptosis in the treatment of SAP. Our study provides new insights and strategies for the application of cell therapy for the treatment of SAP.

Supplementary Information The online version contains supplementary material available at https://doi.org/10.1007/s10495-024-01946-5.

Author contributions S.Lyu: conceptualization, investigation, data collection and curation, and writing of the manuscript. S.Liu: investigation, data curation, and writing of manuscript. X.G.: investigation, software, and data visualization. Y.Z.: technical support, software, and data visualization. Z.L.: data curation, analysis, and visualization. S.S.: investigation, data collection, and software. W.L.: investigation, technical support, and data collection. J.P.: conceptualization, investigation, and technical support. Y.F.: conceptualization, funding acquisition, supervision, project administration, and critical revision and final approval of the manuscript. H.S.: conceptualization, funding acquisition, supervision, project administration, and critical revision and final approval of the manuscript.

Funding This work was supported by the Joint Research Project of The General Hospital of Western Theater Command (Grant No. 2019LH04) and the National Natural Science Foundation of China (Grant No. 81772001).

Data availability No datasets were generated or analysed during the current study.

Declarations

Ethics approval This study was approved by the Ethics Committee of the General Hospital of Western Theater Command of the Chinese People's Liberation Army (2021EC2-20). The researchers strictly followed the Principles of Laboratory Animal Care (revised in 1996) published by the National Institutes of Health of the United States of America and the Animal Management Regulations (revised in 2017) issued by the National Science and Technology Commission of the People's Republic of China to minimize animal suffering and the number of animals used during the experiments.

Competing interests The authors declare no competing interests.

References

1. Schepers NJ et al (2019) Impact of characteristics of organ failure and infected necrosis on mortality in necrotising pancreatitis. Gut 68(6):1044–1051
2. Iyer S et al (2020) Know Thy enemy-understanding the role of inflammation in severe Acute Pancreatitis. Gastroenterology 158(1):46–48
3. Nieminen A et al (2014) Circulating cytokines in predicting development of severe acute pancreatitis. Crit Care 18(3):R104
4. Hines OJ, Pandol SJ (2019) Management of severe acute pancreatitis. BMJ 367:l6227
5. Yi T, Song SU (2012) Immunomodulatory properties of mesenchymal stem cells and their therapeutic applications. Arch Pharm Res 35(2):213–221
6. Murphy MB, Moncivais K, Caplan AI (2013) Mesenchymal stem cells: environmentally responsive therapeutics for regenerative medicine. Exp Mol Med 45(11):e54
7. Wang S et al (2022) Targeted therapy for inflammatory diseases with mesenchymal stem cells and their derived exosomes: from Basic to Clinics. Int J Nanomed 17:1757–1781
8. Huang Q et al (2021) Placental chorionic plate-derived mesenchymal stem cells ameliorate severe acute pancreatitis by

regulating macrophage polarization via secreting TSG-6. Stem Cell Res Ther 12(1):337
9. Meng HB et al (2013) Therapeutic effect of human umbilical cord-derived mesenchymal stem cells in rat severe acute pancreatitis. Int J Clin Exp Pathol 6(12):2703–2712
10. Li Q et al (2018) TSG-6 secreted by human adipose tissue-derived mesenchymal stem cells ameliorates severe acute pancreatitis via ER stress downregulation in mice. Stem Cell Res Ther 9(1):255
11. Saluja A et al (2019) Early intra-acinar events in Pathogenesis of Pancreatitis. Gastroenterology 156(7):1979–1993
12. Gorelick FS, Thrower E (2009) The acinar cell and early pancreatitis responses. Clin Gastroenterol Hepatol 7(11 Suppl):S10–S14
13. Jorgensen I, Miao EA (2015) Pyroptotic cell death defends against intracellular pathogens. Immunol Rev 265(1):130–142
14. Shi J, Gao W, Shao F (2017) Pyroptosis: gasdermin-mediated programmed necrotic cell death. Trends Biochem Sci 42(4):245–254
15. Liu Z et al (2019) Crystal structures of the full-length murine and human gasdermin D reveal mechanisms of autoinhibition, lipid binding, and oligomerization. Immunity 51(1):43–49e4
16. Ding J et al (2016) Pore-forming activity and structural autoinhibition of the gasdermin family. Nature 535(7610):111–116
17. Wang J et al (2021) Cathepsin B aggravates acute pancreatitis by activating the NLRP3 inflammasome and promoting the caspase-1-induced pyroptosis. Int Immunopharmacol 94:107496
18. Gao L et al (2021) Acinar cell NLRP3 inflammasome and gasdermin D (GSDMD) activation mediates pyroptosis and systemic inflammation in acute pancreatitis. Br J Pharmacol 178(17):3533–3552
19. Huang Q et al (2019) An efficient protocol to generate placental chorionic plate-derived mesenchymal stem cells with superior proliferative and immunomodulatory properties. Stem Cell Res Ther 10(1):301
20. Schmidt J et al (1992) A better model of acute pancreatitis for evaluating therapy. Ann Surg 215(1):44–56
21. Hu Q et al (2023) Extracellular vesicle ITGAM and ITGB2 mediate severe Acute pancreatitis-related Acute Lung Injury. ACS Nano 17(8):7562–7575
22. Wei X et al (2022) Role of pyroptosis in inflammation and cancer. Cell Mol Immunol 19(9):971–992
23. Al Mamun A et al (2022) Pyroptosis in acute pancreatitis and its therapeutic regulation. Apoptosis 27(7–8):465–481
24. Wang J et al (2020) CircHIPK3 promotes pyroptosis in Acinar cells through regulation of the miR-193a-5p/GSDMD Axis. Front Med (Lausanne) 7:88
25. Xia S et al (2021) Gasdermin D pore structure reveals preferential release of mature interleukin-1. Nature 593(7860):607–611
26. Song N, Scholtemeijer M, Shah K (2020) Mesenchymal stem cell immunomodulation: mechanisms and therapeutic potential. Trends Pharmacol Sci 41(9):653–664
27. Mishra VK et al (2020) Identifying the therapeutic significance of mesenchymal stem cells. Cells 9(5):1145
28. Langrzyk A et al (2018) Critical view on mesenchymal stromal cells in Regenerative Medicine. Antioxid Redox Signal 29(2):169–190
29. Saadh MJ et al (2023) Therapeutic potential of mesenchymal stem/stromal cells (MSCs)-based cell therapy for inflammatory bowel diseases (IBD) therapy. Eur J Med Res 28(1):47
30. Ma HC et al (2014) Targeted migration of mesenchymal stem cells modified with CXCR4 to acute failing liver improves liver regeneration. World J Gastroenterol 20(40):14884–14894
31. Bedoui Y et al (2020) Emerging roles of Perivascular Mesenchymal Stem cells in synovial joint inflammation. J Neuroimmune Pharmacol 15(4):838–851
32. Szydlak R (2019) Mesenchymal stem cells' homing and cardiac tissue repair. Acta Biochim Pol 66(4):483–489
33. Ge P et al (2020) Intestinal barrier damage, systemic inflammatory response syndrome, and acute lung injury: a troublesome trio for acute pancreatitis. Biomed Pharmacother 132:110770
34. Liu W et al (2021) Liver injury associated with acute pancreatitis: the current status of clinical evaluation and involved mechanisms. World J Clin Cases 9(34):10418–10429
35. Ferrini E et al (2021) Persistency of mesenchymal Stromal/Stem cells in lungs. Front Cell Dev Biol 9:709225
36. Feng Z et al (2022) Mesenchymal stem cells protect against TBI-induced pyroptosis in vivo and *in vitro* through TSG-6. Cell Commun Signal 20(1):125
37. Pan K et al (2023) Temporal patterns and distribution of pyroptosis-related molecules and effects of human mesenchymal stem cells on pyroptosis following cerebral ischemia/reperfusion in rats. J Stroke Cerebrovasc Dis 32(8):107199
38. Zhang X et al (2023) VCAM-1(+) hUC-MSCs exert considerable neuroprotection against cerebral infarction in rats by suppression of NLRP3-Induced pyroptosis. Neurochem Res 48(10):3084–3098
39. Schroder K, Tschopp J (2010) The inflammasomes. Cell 140(6):821–832
40. Swanson KV, Deng M, Ting JP (2019) The NLRP3 inflammasome: molecular activation and regulation to therapeutics. Nat Rev Immunol 19(8):477–489
41. Harrell CR et al (2023) NLRP3 inflammasome as a potentially new therapeutic target of mesenchymal stem cells and their exosomes in the treatment of Inflammatory Eye diseases. Cells 12(18):2327
42. Nazari S et al (2023) Mesenchymal stem cells (MSCs) and MSC-derived exosomes in animal models of central nervous system diseases: targeting the NLRP3 inflammasome. IUBMB Life 75(10):794–810